

# Analysing surface energy balance closure and partitioning over a semi-arid savanna FLUXNET site in Skukuza, Kruger National Park, South Africa

Nobuhle P. Majozi<sup>1,2</sup>, Chris M. Mannaerts<sup>2</sup>, Abel Ramoelo<sup>1,5</sup>, Renaud Mathieu<sup>1,3</sup>, Alecia Nickless<sup>4</sup>, Wouter Verhoef<sup>2</sup>

<sup>1</sup>Earth Observation Group, Natural Resources and Environment, Council for Scientific and Industrial Research, Pretoria, South Africa, 0001

<sup>2</sup>Department of Water Resources, Faculty of Geo-Information Science and Earth Observation (ITC), University of Twente, Enschede, 75AA, the Netherlands

<sup>3</sup>Department of Geography, Geoinformatics and Meteorology, University of Pretoria, South Africa

<sup>4</sup>Nuffield Department of Primary Care Health Sciences, University of Oxford, Oxford, OX2 6GG, United Kingdom

<sup>5</sup>University of Limpopo, Risk and Vulnerability Centre, Sovenga, South Africa, 0727

Correspondence to: N. P. Majozi ([nmajozi@csir.co.za](mailto:nmajozi@csir.co.za))

## Abstract

Flux towers provide essential terrestrial climate, water and radiation budget information needed for environmental monitoring and evaluation of climate change impacts on ecosystems and society in general. They are also intended for calibration and validation of satellite-based earth observation and monitoring efforts, such as assessment of evapotranspiration from land and vegetation surfaces using surface energy balance approaches.

In this paper, 15 years of Skukuza eddy covariance data, i.e. from 2000 to 2014, were analysed for surface energy balance closure (EBC) and partitioning. The surface energy balance closure was evaluated using the ordinary least squares regression (OLS) of turbulent energy fluxes (sensible (H) and latent heat (LE)) against available energy (net radiation (Rn) less soil heat (G)), and the energy balance ratio (EBR). Partitioning of the surface energy during the wet and dry seasons was [also](#) investigated, as well as how it is affected by atmospheric vapor pressure deficit (VPD), and net radiation.

After filtering years with [bad-low quality](#) data (2004-2008), our results show an overall mean EBR of 0.93. Seasonal variations of EBR also showed [summer-wet with 1.17](#) and spring (1.02) [being](#) closest to unity, with [winter-dry](#) (0.70) having the [highest imbalance](#). Nocturnal surface energy closure was very low at 0.26, and this was linked to low friction velocity during night-time, with results showing an increase in closure with increase in friction velocity.

The surface energy partitioning of this savanna ecosystem showed that sensible heat flux dominated the energy partitioning between March and October, followed by latent heat flux, and lastly the soil heat flux, and during the wet season where latent heat flux dominated sensible heat flux. An increase in net radiation was characterized by an increase in both LE and H, with LE showing a higher rate of increase than H in the wet season, and the reverse happening during the dry season. An increase in VPD is [correlated with](#) a decrease in LE and increase in H during the wet season, and an increase of both fluxes during the dry season.

## 1. Introduction

Net solar radiation (Rn) reaching the earth's surface determines the amount of energy available for latent (LE), sensible (H) and soil (G) heat fluxes, and heat stored by the canopy, the ground [and energy storage terms by photosynthesis](#). Energy partitioning on the earth's surface is a function of interactions between biogeochemical cycling, plant physiology, the state of the atmospheric boundary layer and climate (Wilson et al., 2002). How the turbulent fluxes (H and LE) are partitioned in an ecosystem plays a critical role in determining the hydrological cycle, boundary layer development, weather and climate (Falge et al., 2005). Understanding the partitioning of energy, particularly the turbulent fluxes, is important for water resource management in (semi) arid regions, where [potential-reference](#) evapotranspiration far exceeds precipitation.

49 Eddy covariance (EC) systems are currently the most reliable method for measuring carbon, energy and  
50 water fluxes, and they have become a standard technique in the study of surface-atmosphere boundary layer  
51 interactions. They provide a distinct contribution to the study of environmental, biological and climatological  
52 controls of the net surface exchanges between the land surface (including vegetation) and the atmosphere  
53 (Aubinet, et al., 1999; Baldocchi et al., 2001). The accuracy of these data is very important because they are used  
54 to validate and assess performance of land surface and climate models. However, the EC techniques have  
55 limitations in terms of data processing and quality control methods, especially under complex conditions (e.g.,  
56 unfavorable weather, such as high turbulence and low wind speed, and heterogeneous topography). In EC  
57 measurements, the ideal situation is that available energy, i.e. net radiation minus soil heat flux is equal to the sum  
58 of the turbulent fluxes ( $R_n - G = LE + H$ ); however, in most instances, the measured available energy is larger than  
59 the sum of the ~~measurable-measured~~ turbulent fluxes of sensible heat and latent heat. Extensive research on the  
60 issue of surface energy imbalance in EC observations has been done (Barr et al., 2012; Chen et al., 2009; Foken  
61 et al., 2010; Franssen et al., 2010; Mauder et al., 2007), and closure error (or imbalance) has been documented to  
62 be around 10-30 % ([Wilson et al., \(2002\); von Randow et al., \(2004\); Sanchez et al., \(2010\)](#)).

63 Causes for non-closure, [as extensively discussed](#), include unaccounted soil and canopy heat storage  
64 [terms](#), non-inclusion of the low and high frequency turbulence in the computation of the turbulent fluxes, land  
65 surface heterogeneities, systematic measurement and sampling errors. This imbalance has implications on how  
66 energy flux measurements should be interpreted and how these estimates should be compared with model  
67 simulations. The surface energy balance closure is an accepted performance criterion of EC flux data (Twine et  
68 al., 2000; Wilson et al., 2002), and different methods have been used to assess the energy closure and partitioning,  
69 including ordinary least squares regression (OLS) method, i.e. a plot of turbulence fluxes ( $H + LE$ ) against available  
70 energy ( $R_n - G$ ), the residual method, i.e.  $R_n - G - H - LE$ , and the energy balance ratio, i.e.  $(H + LE) / (R_n - G)$ .

71 Several researchers have investigated surface energy partitioning and energy balance closure for different  
72 ecosystems, including savannas. Bagayoko et al. (2007) examined the seasonal variation of the energy balance in  
73 West African savannas, and noted that latent heat flux played a major role in the wet season, whereas sensible  
74 heat flux was significant in the dry season. In the grassland Mongolian Plateau, Li et al. (2006) concluded that  
75 sensible heat flux dominated the energy partitioning, followed by ground heat flux, with the rainy season showing  
76 slight increase in latent heat flux. Gu et al. (2006) used different ratios (Bowen ratio,  $G/R_n$ ,  $H/R_n$  and  $LE/R_n$ ) to  
77 investigate surface energy exchange in the Tibetan Plateau, and showed that during the vegetation growth period,  
78  $LE$  was higher than  $H$ , and this was reversed during the post-growth period.

79 Research using the Skukuza EC system data has focused mainly on the carbon exchange, fire regimes, and  
80 in global analysis of the energy balance (Archibald et al., 2009; Kutsch et al., 2008; Williams et al., 2009).  
81 However, there has been no investigation of surface energy partitioning and energy balance closure in this  
82 ecosystem. In this study, we examined the surface energy balance partitioning into soil heat conduction,  
83 convection (sensible) and latent heat components and its energy balance closure using 15 years (2000-2014) of  
84 eddy covariance data from the Skukuza flux tower.

85 First, a multi-year surface energy balance closure (EBC) analysis was done, including the seasonal and day-  
86 night EBC evaluations, and an assessment of its error sources. This included investigating how friction velocity  
87 affects the closure, and its link to low nighttime EBC. [Then, we examined how the surface energy partitioning](#)  
88 [varies with time in this ecosystem, based on the weather conditions in the region, particularly, in relation to water](#)

89 [availability \(precipitation\) and vegetation dynamics. The effect of VPD and Rn on the energy partitioning between](#)  
90 [turbulent fluxes](#) during the wet and dry seasons was [also](#) examined. [Through this study, we expect to contribute](#)  
91 [to existing literature on the surface energy balance closure and partitioning, especially in savanna sites.](#)

## 93 2. Materials and methods

### 94 2.1. Site description

95 The Skukuza flux tower (25.02°S, 31.50°E) was established early 2000 as part of the SAFARI 2000 campaign  
96 and experiment, set up to understand the interactions between the atmosphere and the land surface in Southern  
97 Africa by connecting ground data of carbon, water, and energy fluxes with remote sensing data generated by Earth  
98 observing satellites (Scholes et al., 2001; Shugart et al., 2004).

99 The site is located in the Kruger National Park (South Africa) at 365 m above sea level, and receives 550  
100 ± 160 mm precipitation per annum between November and April, with significant inter-annual variability. The  
101 year is divided into a hot, wet growing season and a warm, dry non-growing season. The soils are generally  
102 shallow, with coarse sandy to sandy loam textures (about 65 % sand, 30 % clay and 5% silt). The area is  
103 characterized by a catenal pattern of soils and vegetation, with broad-leaved *Combretum* savanna on the crests  
104 dominated by the small trees (*Combretum apiculatum*), and fine-leaved *Acacia* savanna in the valleys dominated  
105 by *Acacia nigrescens* (Scholes et al., 1999). The vegetation is mainly open woodland, with approximately 30 %  
106 tree canopy cover of mixed *Acacia* and *Combretum* savanna types. Tree canopy height is 5–8 m with occasional  
107 trees (mostly *Sclerocarya birrea*) reaching 10 m. The grassy and herbaceous understory comprises grasses such  
108 as *Panicum maximum*, *Digitaria eriantha*, *Eragrostis rigidor*, and *Pogonarthria squarrosa*.

#### 109 110 2.1.1. Eddy covariance system

111 Since 2000, ecosystem-level fluxes of water, heat and carbon dioxide are measured using an eddy covariance  
112 system mounted at 16 m height of the 22 m high flux tower. The measurements taken and the instruments used  
113 are summarized in Table 1.

##### 114 (Table 1)

115 From 2000 to 2005, H and LE were derived from a closed-path CO<sub>2</sub>/H<sub>2</sub>O monitoring system, which was replaced  
116 by the open-path gas analyzer in 2006. Also, from 2000 to 2008, incident and reflected shortwave radiation (i.e.  
117 300–1100 nm, Wm<sup>-2</sup>), incident and reflected near-infrared (600–1100 nm, Wm<sup>-2</sup>) and incoming and emitted  
118 longwave radiation (>3.0 μm, Wm<sup>-2</sup>) measurements were made using a two-component net radiometer (Model  
119 CNR 2: Kipp & Zonen, Delft, The Netherlands) at 20 s intervals and then recorded in the data-logger as 30 min  
120 averages; this was replaced with the Kipp & Zonen NRLite net radiometer in 2009. Soil heat flux is measured  
121 using the HFT3 plates (Campbell Scientific) installed at 5 cm below the surface at three locations, two under tree  
122 canopies and one between canopies.

123 Ancillary meteorological measurements include air temperature and relative humidity, also measured at  
124 16 m height, using a Campbell Scientific HMP50 probe; precipitation at the top of the tower using a Texas  
125 TR525M tipping bucket rain gauge; wind speed and direction using a Climatronics Wind Sensor; and soil  
126 temperature using Campbell Scientific 107 soil temperature probe.

128 **2.1.2. Data pre-processing**

129 The Eddysoft software was used to process the raw data collected from the eddy covariance system (Kolle &  
130 Rebmann, 2007). Post-processing of the raw high frequency (10 Hz) data for calculation of half-hour periods of  
131 the turbulent fluxes and CO<sub>2</sub> (F<sub>c</sub>; g CO<sub>2</sub> m<sup>-2</sup> time<sup>-1</sup>) involved standard spike filtering, planar rotation of velocities  
132 and lag correction to CO<sub>2</sub> and q (Aubinet et al., 1999; Wilczak et al., 2001). Frequency response correction of  
133 some of the energy lost due to instrument separation, tube attenuation, and gas analyzer response for LE and F<sub>c</sub>  
134 was performed with empirical co-spectral adjustment to match the H co-spectrum (Eugster and Senn, 1995; Su et  
135 al., 2004).

136

137 **2.2. Data analysis**

138 Half-hourly measurements of eddy covariance and climatological data from 2000 to 2014 were used to assess  
139 surface energy partitioning and closure. When measuring the different variables, instruments like the sonic  
140 anemometer and the net radiometer are affected by different phenomena, like rainfall events and wind gusts,  
141 resulting in faulty diagnostic signals, outliers and data gaps, which are sources of error and bias. Thus cleaning,  
142 which involved screening, diagnosing and editing, of these half-hourly surface energy data, which was done to  
143 reduce bias and error, rejected i) data from periods of sensor malfunction (i.e. when there was a faulty diagnostic  
144 signal), (ii) incomplete 30-minute datasets of R<sub>n</sub>, G, LE and H, and iii) outliers. The data outliers were detected  
145 using the outlier detection procedure found in the Statistica software. After data screening, flux data with non-  
146 missing values of R<sub>n</sub>, G, LE and H data were arranged according to monthly and seasonal periods (summer  
147 (December – February), autumn (March – May), winter (June – August), and spring (September – November)),  
148 as well as into daytime and nighttime.

149 Soil heat flux was then computed as a weighted mean of the three measurements, i.e., two taken under  
150 tree canopies and one on open space.

151

152 **2.2.1. Surface energy balance assessment**

153 The law of conservation of energy states that energy can neither be created nor destroyed, but is transformed from  
154 one form to another, hence the ideal surface energy balance equation is written as:

155 
$$Rn - G = H + LE \tag{1}$$

156 Energy imbalance occurs when both sides of the equation do not balance. The energy balance closure was  
157 evaluated at different levels, i.e. multi-year, seasonal, and day/ night periods (the assumption being that daytime  
158 has positive R<sub>n</sub> and nighttime has negative R<sub>n</sub>), using two methods, i.e.

159 i) The ordinary least squares method (OLS), which is the regression between turbulent fluxes and available  
160 energy.

161 Ideal closure is when the intercept is zero and slope and the coefficient of determination (R<sup>2</sup>) are one. An  
162 assumption is made using this method, that there are no random errors in the independent variables, i.e. R<sub>n</sub> and  
163 G, which of course is an incorrect assumption a simplification.

164 ii) The energy balance ratio (EBR), which is ratio of the sum of turbulent fluxes to the available energy,  
165 
$$\Sigma(LE + H) / \Sigma(Rn - G).$$

166 The EBR gives an overall evaluation of energy balance closure at longer time scales by averaging over errors in  
167 the half-hour measurements; and the ideal closure is 1. EBR has the potential to remove biases in the half-hourly

168 data, such as the tendency to overestimate positive fluxes during the day and underestimate negative fluxes at  
169 night. We did not account for the heat storage terms in the EBR, including soil and canopy heat storage, and  
170 energy storage by photosynthesis and respiration, in this study. The significance of neglecting these storage terms  
171 will be discussed.

172 To investigate the effect of friction velocity on EBR and how it is related to time of day, using friction  
173 velocity, the half-hourly data were separated into four 25-percentiles, and the EBR and OLS evaluated. Matlab  
174 was used to create the graphs.

### 176 2.2.2. Analyzing surface energy partitioning

177 To evaluate solar radiation variation and partitioning into latent and sensible heat fluxes in this biome, EC surface  
178 energy data from 2000 to 2014 were used. Violations in micrometeorological assumptions, instrument  
179 malfunction and poor weather result in a proportion of the data being rejected. Yet, our aim was to construct  
180 continuous records of half-hourly fluxes measured by eddy covariance and compute monthly, seasonal and annual  
181 sums of surface energy fluxes. To fill the gaps in our dataset, we used the Amelia II software, an R-program  
182 designed to impute missing data using Expectation-Maximization with Bootstrapping (EMB) multiple imputation  
183 algorithm (Honaker et al., 2011). The original dataset is resampled using bootstrapping, after which the missing  
184 data values are imputed using Expectation-Maximization algorithm. Each complete imputed dataset is in such a  
185 way that the observed values are the same as those in the original data set; only the missing values are different.

186 The minimum, maximum and mean statistics of Rn, H, LE and G were then estimated. The monthly and  
187 seasonal trends of energy partitioning were assessed, and how each component is affected by vegetation dynamics  
188 at the site. Surface energy partitioning was also characterized as a direct function of vapor pressure deficit (VPD)  
189 and Rn during the wet and dry seasons, following Gu et al. (2006).

## 191 3. Results and Discussion

### 192 3.1. Meteorological conditions

193 Fig 1 shows the 15-year average-daily mean monthly anomalies of air temperature, VPD and rainfall totals at the  
194 Skukuza flux tower site. The annual average temperatures over the 15-year period ranged between 21.13°C in  
195 2012 and 23.23 °C in 2003, with a 15-year average temperature of 22.9 °C. While 2003 was the hottest year, it  
196 was also the driest year, with annual rainfall of 273.6 mm, with 2002 also recording very low rainfall of 325.4  
197 mm, both receiving rainfall amounts below the recorded mean annual rainfall of 550±160 mm. The wettest years  
198 were 2013, 2000, 2014 and 2004 which received 1414, 1115.6, 1010.2 and 1005.7 mm, respectively. 2007 and  
199 2008 had incomplete rainfall data records to assess their annuals. The annual daily average VPD was between  
200 0.024 and 4.03 kPa, with an overall average of 1.28 ± 0.62 kPa. The daily average VPD decreased with rainy  
201 days, and showed an increase during rain-free days. The wet years, i.e. 2000, 2013 and 2014 had low annual  
202 average VPD of 1.98, 1.34 and 1.83 kPa, respectively, whereas the drought years exhibited high VPDs with 2002  
203 and 2003 with 2.77 and 2.97 kPa, respectively. The long-term weather records are comparable with the 1912 –  
204 2001 and 1960 – 1999 climate analysis for the same area as reported by Kruger et al. (2002) and Scholes et al.  
205 (2001), showing a mean annual total precipitation of 547.1 mm and air temperature of 21.9 °C. The low rainfall  
206 during 2000-2003 seasons was also reported by Kutch et al. (2008), who were investigating the connection  
207 between water relations and carbon fluxes during the mentioned period.

208 (Figure 1)

209

## 210 3.2. Surface energy balance assessment

211 Data completeness varied largely 7.59 % (2006) and 67.97 % (2013), with a mean of 34.84 %. The variation in  
212 data completeness is due to a number of factors including instrument failures, changes and (re)calibration, and  
213 poor weather conditions.

214

### 215 3.2.1. Multi-year analysis of surface energy balance closure

216 Fig 2 summarizes results of the multi-year energy balance closure analysis for the Skukuza eddy covariance  
217 system from 2000 to 2014. The coefficient of determination ( $R^2$ ) for the 15-years period varied between 0.74 and  
218 0.92, with a mean value of  $0.85 \pm 0.06$ . The slopes ranged between 0.56 and 1.25, with a mean  $0.77 \pm 0.19$ , while  
219 the intercepts varied from -23.73 to 26.28, with a mean of 1.03 ~~with-and~~ standard deviation of  $18.20 \text{ Wm}^{-2}$ . The  
220 annual energy balance ratio (EBR) for the 15 years extended between 0.44 in 2005 and 2007 and 1.09 in 2011,  
221 with a mean of  $0.78 \pm 0.24$ . Between 2004 and 2008, EBR ranged ~~s~~ between 0.44 and 0.53, whereas from 2000 to  
222 2003 and 2009 to 2014, the EBR ranged-was between 0.76 and 1.09. The EBR for 2010 to 2012 were slightly  
223 greater than 1 (1.08, 1.09 and 1.01, respectively), indicating an overestimation of the turbulent fluxes (H+LE)  
224 compared to the available energy, this still giving the absolute imbalance values of within 30 %. The remaining  
225 years, 2000-2003 and 2009, were less than 1, indicating that the turbulent fluxes were lower than the available  
226 energy. The further away the slope is from unity, the lower the EBR, as shown by the low slope values between  
227 2004 and 2008. The period of low EBR between 2004 and 2008 is characterized by the absence of negative values  
228 of available energy ( $R_n - G$ ) as illustrated in Fig 2. Between 2000 and 2004, the CNR2 net radiometer was used to  
229 measure long and shortwave radiation, and these were combined to derive  $R_n$ . However, when the pyrgeometer  
230 broke down in 2004,  $R_n$  was derived from measured shortwave radiation and modelled longwave radiation until  
231 the CNR2 was replaced by the NRLite net radiometer in 2009. This was a significant source of error, as shown  
232 by the low EBR between 2004 and 2008. The closed-path gas analyzer was also changed to open-path gas analyzer  
233 in 2006. An analysis of the 2006 data (which had very low data completeness of 7.59 %) showed that there were  
234 no measurements recorded until September, possibly due to instrument failure. Further analysis and discussion of  
235 the EBR was done with the exclusion of years with low quality data.

236 Our final mean multiyear EBR estimate, excluding the years with poor data quality (2004 to 2008), was  
237 therefore  $0.93 \pm 0.11$ , ranging between 0.76 and 1.09. The  $R^2$  for these years varied between 0.77 and 0.92, with  
238 a mean value of  $0.87 \pm 0.05$ . The slopes were from 0.7 to 1.25, with a mean  $0.87 \pm 0.17$ , while the intercepts varied  
239 from -12.57 to 26.28, with a mean of 10.79 and standard deviation of  $13.67 \text{ Wm}^{-2}$ .

240 (Figure 2)

241 The EBR results for the Skukuza eddy covariance system, which vary between 0.76 and 1.09 with an annual mean  
242 of 0.93 (only the years with high quality data), are generally within the reported accuracies as shown in most  
243 studies that report the energy balance closure error at 10–30% , across different ecosystems. For instance, Wilson  
244 et al., (2002) also recorded an annual mean EBR of 0.84, ranging between 0.34 and 1.69 in an extensive study  
245 investigating 22 FLUXNET sites across the globe; EBR in ChinaFLUX sites ranged between 0.58 and 1.00, with  
246 a mean of 0.83 (Yuling et al., 2005); according to Were et al. (2007), ~~reported~~ EBR values of about 0.90 were  
247 found over shrub and herbaceous patches, in a dry valley in southeast Spain, ~~whereas~~ Chen et al. (2009) ~~report~~  
248 showed a mean of 0.98 EBR for their study in the semi-arid region of Mongolia, and an EBR value of 0.80 was

249 found by Xin and Liu (2010) in a maize crop in semi-arid conditions, in China. Using data from the Tibetan  
250 Observation and Research Platform (TORP), Liu et al. (2011) observed an EBR value of 0.85 in an alfalfa field  
251 in semi-arid China.

### 252 253 **3.2.2. Seasonal variation of EBR**

254 Fig 3 shows the seasonal OLS results for the 15 year period, excluding years 2004 to 2008. The slopes ranged  
255 between 0.94~~67~~ and 1.21~~0.87~~, with a mean of  $1.10 \pm 0.11$  0.78 $\pm$ 0.08, and the intercepts were a mean of ~~11.97~~19.13  
256  $\text{Wm}^{-2} \pm 3.87$  16.30  $\text{Wm}^{-2}$ .  $R^2$  ranged between 0.81 and 0.88 with a mean of  $0.84 \pm 0.04$ . The EBR for the different  
257 seasons ranged between 0.70 and 1.12, with a mean of  $0.92 \pm 0.19$ . The winter-dry season had the lowest EBR of  
258 0.70, while summer recorded 1.02, and spring were closest to unity with EBR of ~~-~~and 1.12, respectively, and  
259 autumn had EBR of 0.84. A large number of outliers is observed in summer due to cloudy weather conditions and  
260 rainfall events that make the thermopile surface wet, thus reducing the accuracy of the net radiometer. A study  
261 comparing different the performance of different net radiometers by Blonquist et al. (2009) shows that the NR-  
262 Lite is highly sensitive to precipitation and dew/ frost since ~~it~~the sensor is not protected.

263 **(Figure 3)**

264 The results of our study concur with similar studies that assessed the seasonal variation of EBR. For instance,  
265 Wilson et al. (2002) comprehensively investigated the energy closure of the summer and winter seasons for 22  
266 FLUXNET sites for 50 site-years. They also reported higher energy balance correlation during the wet compared  
267 to the dry season, with the mean  $R^2$  of 0.89 and 0.68, respectively. Whereas our results show significant differences  
268 between the wet (1.12) and dry (0.70)-their, their EBR showed smaller differences between the two seasons, being  
269 0.81 and 0.72, for summer and winter, respectively. Ma et al. (2009) reported an opposite result from the Skukuza  
270 results, showing energy closures of 0.70 in summer and 0.92 in winter over the flat prairie on the northern Tibetan  
271 Plateau.

### 272 273 **3.2.3. Day – night-time effects**

274 Fig 4 shows the daytime and nocturnal OLS regression results for the 15 year period. The daytime and nocturnal  
275 slopes were 0.99 and 0.11, with the intercepts being 76.76 and 1.74  $\text{Wm}^{-2}$ , respectively. Daytime and nocturnal  
276  $R^2$  were 0.64 and 0.01, respectively. The EBR for the different times of day were 0.96 and 0.27, daytime and  
277 nocturnal, respectively.

278 **(Figure 4)**

279 Other studies also reported a higher daytime surface energy balance closure. For instance, Wilson et al., (2002)  
280 showed that the mean annual daytime EBR was 0.8, whereas the nocturnal EBR was reported to be was negative  
281 or was much less or much greater than 1.

282 To understand the effect of friction velocity on the energy balance closure, surface energy data which  
283 had corresponding friction velocity ( $u^*$ ) data, were analysed~~used~~. Using friction velocity, the data were separated  
284 into four 25-percentiles, and the EBR and OLS evaluated. Results show that the first quartile, the EBR was 3.94,  
285 with the 50-percentile at 0.99, the third quartile at unity, and the fourth quartile at 1.03 (Fig 5). The slopes were  
286 between 1.01 and 1.12, with the intercepts ranging between -9.26 and -0.17  $\text{Wm}^{-2}$ , whereas  $R^2$  were 0.82, 0.86,  
287 0.85 and 0.81 for the first to the fourth quartiles, respectively.

288 **(Figure 5)**

289 An assessment shows that the time associated with the low friction velocities, i.e. the first quartile are night-time  
290 data constituting 81 % of the whole first quartile dataset, and the last quartile had the highest number of daytime  
291 values at 79.29 % of the fourth quartile dataset. Lee and Hu (2002) hypothesized that the lack of energy balance  
292 closure during nocturnal periods was often the result of mean vertical advection, whereas Aubinet et al.,  
293 (1999) and Blanken et al., (1997) showed that energy imbalance during nocturnal periods is usually greatest when  
294 friction velocity is small. Another source of error in the nocturnal EBR is the high uncertainty in night-time  
295 measurements of  $R_n$ . At night, the assumption is that there is no shortwave radiation, and  $R_n$  is a product of  
296 longwave radiation. Studies show that night-time measurements of longwave radiation were less accurate than  
297 daytime measurements (Blonquist et al., 2009). The RN-Lite, for instance has low sensitivity to longwave  
298 radiation, resulting in low accuracy in low measurements.

299 Soil heat flux (G) plays a significant role in the surface energy balance as it determined how much energy  
300 is available for the turbulent fluxes, especially in areas with limited vegetation cover. In this study, we examined  
301 how G, i.e., its presence or absence, impacts on the EBR. Our results revealed a decrease of up to 7 %, with an  
302 annual mean of  $3.13 \pm 2.70$ , in EBR when G was not included in the calculation. During the daytime, the absence  
303 of G resulted in a decrease of approximately 10 % of the initial EBR, while at nighttime EBR was as low as 50 %  
304 of the initial EBR, showing that G has greater impact on the surface energy balance at night. While G plays a  
305 significant role on the surface energy balance closure, our study ignored the different energy storage terms in  
306 determining the EBR, including the soil heat storage term. The exclusion of this storage term results in the  
307 underestimation of G, as the real value of G is a combination of the flux measured by the plate and the heat  
308 exchange between the ground and the depth of the plate. This in turn contributes to overestimating the available  
309 energy, which then lowers the EBC. As reported by different studies, the omission of the soil heat storage results  
310 in the underestimation of the energy EBC by up to 7 %. For instance, Zuo et al. (2011) reported an improvement  
311 of 6 to 7 % when they included the soil heat storage in their calculation of EBR., at the Semi-Arid Climate and  
312 Environment Observatory of Lan-Zhou University (SACOL) site in semi-arid grassland over the Loess Plateau  
313 of China. In their study in the three sites in the Badan Jaran desert, Li, Liu, Wang, Miao, and Chen (2014) analysed  
314 the effect of including soil heat storage derived by different methods in the energy balance closure; their EBR  
315 improved by between 1.5 % and 4 %. The improvement of the EBR in the study in a FLUXNET boreal site in  
316 Finland by Sánchez, Caselles, and Rubio (2010) was shown to be 3 % when the soil heat storage was included,  
317 which increased to 6 % when other storage terms (canopy air) were taken into account.

### 319 3.3. Surface energy partitioning

#### 320 3.3.1. Surface energy measurements

321 The mean daily and annual measurements of the energy budget components from 2000 to 2014 are highlighted in  
322 Fig 6 and Table 2. The seasonal cycle of each component can be seen throughout the years, where at the beginning  
323 of each year the energy budget components are high, and as each year progresses they all decrease to reach a low  
324 during the middle of the year, which is the winter/ dry season, and a gradual increase being experienced during  
325 spring right to the summer at the end of each year. The multi-year daily means of  $R_n$ , H, LE and G were  $139.1$   
326  $Wm^{-2}$ ,  $57.70 Wm^{-2}$ ,  $42.81 Wm^{-2}$  and  $2.94 Wm^{-2}$ , with standard deviations of  $239.75 Wm^{-2}$ ,  $104.15 Wm^{-2}$ ,  $70.58$   
327  $Wm^{-2}$  and  $53.67 Wm^{-2}$ , respectively.

328 (Figure 6)



329 The gaps in 2006 indicate the absence of the surface energy flux measurements in those years, which was a result  
330 of instrument failure. Between 2004 and 2008, the Rn was calculated as a product of measured shortwave radiation  
331 and modelled longwave radiation, which was a high source of error in the estimation of Rn. These years are also  
332 ~~characterised~~characterized by poor energy balance closure, as shown in Section 3.2.1 above.

333 (Table 2)

334

### 335 3.3.2. Influence of weather conditions and seasonality

336 In arid/semi-arid ecosystems, solar radiation is not a limiting factor for latent heat flux, instead it is mainly limited  
337 by water availability. The seasonal fluctuations of energy fluxes are affected by the seasonal changes in the solar  
338 radiation, air temperature, precipitation and soil moisture (Baldocchi et al., 2000; Arain et al., 2003). These  
339 climatic variables influence vegetation dynamics in an ecosystem, as well as how solar radiation is partitioned.  
340 Hence, daily measurements of precipitation, air temperature and VPD were evaluated to investigate the  
341 partitioning of the surface energy in the semi-arid savanna landscape of Skukuza.

342 (Figure 7)

343 To illustrate the partitioning of solar radiation into the different fluxes throughout the year, Fig 7 presents  
344 the multi-year mean monthly variations of the surface energy components showing a general decrease of the  
345 components between February and June, which then gradually increases again until November. The multi-year  
346 monthly means of Rn, H, LE and G were 71.27 Wm<sup>-2</sup> (June) and 197.33 Wm<sup>-2</sup> (November), 37.11 Wm<sup>-2</sup> (June)  
347 and 80.37 Wm<sup>-2</sup> (November), 8.52 Wm<sup>-2</sup> (August) and 127.17 Wm<sup>-2</sup> (December), -2.28 Wm<sup>-2</sup> (June) and 20.78  
348 Wm<sup>-2</sup> (November), respectively. The month of August had the highest BR of 6.42, whereas December had the  
349 least at 0.42. The residual accounted for between ~~-19.69 and~~ 34.74 % of Rn, and an average of 4.70 %.

350 The general trend shows that sensible heat flux dominated the energy partitioning between May and  
351 October, followed by latent heat flux, and lastly the soil heat flux, except during the wet season where latent heat  
352 flux was larger than sensible heat flux. This is illustrated by the trend of BR, showing an increase from April, with  
353 the peak in August, then a steady decrease until it hits lowest in December. The period of low BR is  
354 ~~characterised~~characterized by high Rn and high precipitation. As the season transitions into ~~winter~~the dry season,  
355 it is ~~characterised~~characterized by reduced net radiation and low measurements H and LE.

356 Just before the first rains, i.e. between September and November, tree flowering and leaf emergence  
357 occurs in the semi-arid savanna in the Skukuza area (Archibald and Scholes, 2007), and grasses shoot as soil  
358 moisture availability improves with the rains (Scholes et al., 2003). This is ~~characterised~~characterized by a gradual  
359 increase in LE and decrease in BR, which, when compared to the ~~winter-dry~~ season, is significantly lower than  
360 the H, as illustrated in Fig 7. As the rainy season progresses, and vegetation development peaks, LE also reaches  
361 its maximum, becoming significantly higher than H, and hence, low BR. Between March and September, when  
362 leaf senescence occurs, the leaves gradually change colour to brown and grass to straw, and trees defoliate, H  
363 again gradually becomes significantly higher than LE.

364 (Figure 8)

365 The influence of VPD and Rn on surface energy partitioning was investigated during the wet and dry  
366 seasons. Results show that during both periods there is an increase in H and decrease in LE with an increase in  
367 VPD: although the gradient of LE decrease differ significantly during the two periods, H increases similarly during  
368 both the wet and dry periods (Fig 89). VPD is higher in times of little or no rain (low soil water availability),

369 which explains the decrease in LE with a rise in VPD. In this instance, although the evaporative demand is high,  
370 the stomatal conductance is reduced due to absence of water in the soil, resulting in smaller LE and higher H. Rn,  
371 on the other hand, is partitioned into different fluxes, based on other climatic and vegetation physiological  
372 characteristics. Fig 9 illustrates that both LE and H increase with increase in Rn, although their increases are not  
373 in proportion, based on season. During the wet season, the rate of increase of LE is higher than that of H, whereas  
374 in the dry season the reverse is true. The rate of increase of LE is controlled by the availability of soil water  
375 (precipitation), (also illustrated in Fig\_6 (LE)), and during the wet season it increases steadily with increasing Rn,  
376 whereas the rate of increase of H is concave, showing saturation with an increase in Rn. The opposite is true  
377 during the dry season, with limited water availability, where the rate of increase of LE slows down with increase  
378 in Rn, and a steady increase of H with Rn increase.

#### 379 **(Figure 9)**

380 Our study results are consistent with similar studies, for exampleGu, Gu et al. (2006), who examined  
381 how soil moisture, vapor pressure deficit (VPD) and net radiation control surface energy partitioning at a  
382 temperate deciduous forest site in central Missouri, USA. Both studies agree that with ample soil moisture, during  
383 the rainy season, latent heat flux dominates over sensible heat flux, and reduced soil water availability reversed  
384 the dominance of latent heat over sensible heat, because of its direct effect on stomatal conductance. An increase  
385 in net radiation, on the other hand, also increases both sensible and latent heat fluxes. The increase of either then  
386 becomes a function of soil moisture availability, since they cannot increase in the same proportion. However,  
387 whereas we found that a rise in VPD is characterized by a decrease in LE and an increase in H in both periods,  
388 their findings show a significant increase in LE and decrease in H with a rise in VPD during the non-drought  
389 period, with both components showing slight increases with increase in VPD in dry conditions. Li et al. (2012)  
390 also investigated the partitioning of surface energy in the grazing lands of Mongolia, and concluded that the energy  
391 partitioning was also controlled by vegetation dynamics and soil moisture availability, although soil heat flux is  
392 reportedly higher than latent heat flux in most instances. In a temperate mountain grassland in Austria, Hammerle  
393 et al., (2008) found that the energy partitioning in this climatic region was dominated by latent heat flux, followed  
394 by sensible heat flux and lastly soil heat flux.

395 The consensus in all above studies is that vegetation and climate dynamics play a critical role in energy  
396 partitioning. They note that during full vegetation cover, latent heat flux is the dominant portion of net radiation.  
397 However, depending on the climatic region, the limiting factors of energy partitioning vary between water  
398 availability and radiation. Our study confirms that in semi-arid regions, sensible heat flux is the highest fraction  
399 of net radiation throughout the year, except during the wet period, when latent heat flux surpasses sensible heat  
400 flux. However, in regions and locations where water availability is not a limiting factor, latent heat flux may take  
401 the highest portion of net radiation.

#### 402 403 **4. Conclusion**

404 This study investigated both surface energy balance and ~~its-how it is partitioning-partitioned~~ into turbulent fluxes  
405 during the wet and dry seasons in a semi-arid savanna ecosystem in Skukuza using eddy covariance data from  
406 2000 to 2014. The analysis revealed a mean multi-year energy balance ratio of 0.93, ~~The~~the variation of RBR  
407 based on season, time of day and as a function of friction velocity was explored. The seasonal EBR varied between  
408 0.70 and 1.12, with ~~winter-the dry season~~ recording the highest energy imbalance. Daytime EBR was as high as

409 0.96, with 0.27 EBR for the nighttime. The high energy imbalance at night was explained as a result of stable  
410 conditions, which limit turbulence that is essential for the creation of eddies. The assessment of the effect of  
411 friction velocity on EBR showed that EBR increased with an increase in friction velocity, with low friction  
412 velocity experienced mainly during night-time.

413 The energy partition analysis revealed that sensible heat flux is the dominant portion of net radiation in  
414 this semi-arid region, except ~~in summer, when there is rainfall~~during the rainfall period. The results also show  
415 that water availability and vegetation dynamics play a critical role in energy partitioning, whereby when it rains,  
416 vegetation growth occurs, leading to an increase in latent heat flux / evapotranspiration. Clearly an increase in Rn  
417 results in a rise in H and LE, however their increases are controlled by water availability. During the wet season,  
418 the rate of increase of LE is higher than that of H, whereas in the dry season the reverse is true. The rate of increase  
419 of LE is controlled by the availability of soil water (precipitation), and during the wet season it increases steadily  
420 with increasing Rn, whereas the rate of increase of H shows saturation with an increase in Rn. The opposite is  
421 true during the dry season, with limited water availability, the rate of increase of LE reaches saturation with  
422 increase in Rn and a steady increase of H with Rn increase. An increase in VPD, on the other hand, results in an  
423 increase in H and decrease in LE, with higher VPD experienced during the dry season, which explains the high  
424 H, although the evaporative demand is high.

425

#### 426 **Acknowledgements**

427 This study was supported by the Council for Scientific and Industrial Research under the project entitled  
428 “Monitoring of water availability using geo-spatial data and earth observations”, and the National Research  
429 Foundation under the Thuthuka PhD cycle grant.

430

#### 431 **References**

432 Archibald, S., & Scholes, R. (2007). Leaf green-up in a semi-arid ~~afriean~~African savanna-separating tree and grass  
433 responses to environmental cues. *Journal of Vegetation Science*, 18(4), 583-594.

434 Archibald, S., Kirton, A., Merwe, M., Scholes, R., Williams, C., & Hanan, N. (2009). Drivers of inter-annual  
435 variability in net ecosystem exchange in a semi-arid savanna ecosystem, South ~~afriean~~Africa. *Biogeosciences*, 6(2),  
436 251-266.

437 Aubinet, M., Grelle, A., Ibrom, A., Rannik, Ü., Moncrieff, J., Foken, T., . . . Bernhofer, C. (1999). Estimates of  
438 the annual net carbon and water exchange of forests: The EUROFLUX methodology. *Advances in Ecological  
439 Research*, 30, 113-175.

440 Bagayoko, F., Yonkeu, S., Elbers, J., & van de Giesen, N. (2007). Energy partitioning over the West African  
441 savanna: Multi-year evaporation and surface conductance measurements in eastern ~~burkina~~Burkina fasoFaso.  
442 *Journal of Hydrology*, 334(3), 545-559.

443 Baldocchi, D., Falge, E., Gu, L., Olson, R., Hollinger, D., Running, S., . . . Evans, R. (2001). FLUXNET: A new  
444 tool to study the temporal and spatial variability of ecosystem-scale carbon dioxide, water vapor, and energy flux  
445 densities. *Bulletin of the American Meteorological Society*, 82(11), 2415-2434.

446 Barr, A. G., van der Kamp, G., Black, T. A., McCaughey, J. H., & Nesic, Z. (2012). Energy balance closure at  
447 the BERMS flux towers in relation to the water balance of the White Gull Creek watershed 1999–2009.  
448 *Agricultural and Forest Meteorology*, 153(0), 3-13.

449 Blanken, P., Black, T. A., Yang, P., Neumann, H., Nesic, Z., Staebler, R., . . . Lee, X. (1997). Energy balance and  
450 canopy conductance of a boreal aspen forest: Partitioning overstory and understory components. *Journal of*  
451 *Geophysical Research: Atmospheres* (1984–2012), 102(D24), 28915-28927.

452 Blonquist, J., et al. (2009). "Evaluation of measurement accuracy and comparison of two new and three traditional  
453 net radiometers." *Agricultural and Forest Meteorology* **149**(10): 1709-1721.

454 Chen, S., Chen, J., Lin, G., Zhang, W., Miao, H., Wei, L., . . . Han, X. (2009). Energy balance and partition in  
455 inner Mongolia steppe ecosystems with different land use types. *Agricultural and Forest Meteorology*, 149(11),  
456 1800-1809.

457 Eugster, W., & Senn, W. (1995). A cospectral correction model for measurement of turbulent NO<sub>2</sub> flux. *Boundary-*  
458 *Layer Meteorology*, 74(4), 321-340.

459 Falge, E., Reth, S., Brüggemann, N., Butterbach-Bahl, K., Goldberg, V., Oltchev, A., . . . Queck, R. (2005).  
460 Comparison of surface energy exchange models with eddy flux data in forest and grassland ecosystems of  
461 ~~germany~~Germany. *Ecological Modelling*, 188(2), 174-216.

462 Foken, T., Mauder, M., Liebethal, C., Wimmer, F., Beyrich, F., Leps, J., . . . Bange, J. (2010). Energy balance  
463 closure for the LITFASS-2003 experiment. *Theoretical and Applied Climatology*, 101(1-2), 149-160.

464 Franssen, H., Stöckli, R., Lehner, I., Rotenberg, E., & Seneviratne, S. (2010). Energy balance closure of eddy-  
465 covariance data: A multisite analysis for ~~european~~European FLUXNET stations. *Agricultural and Forest*  
466 *Meteorology*, 150(12), 1553-1567.

467 Goosse H., P.Y. Barriat, W. Lefebvre, M.F. Loutre and V. Zunz, (2008-2010). Introduction to climate dynamics  
468 and climate modeling. Online textbook available at <http://www.climate.be/textbook>.

469 Gu, L., Meyers, T., Pallardy, S. G., Hanson, P. J., Yang, B., Heuer, M., . . . Wullschleger, S. D. (2006). Direct  
470 and indirect effects of atmospheric conditions and soil moisture on surface energy partitioning revealed by a  
471 prolonged drought at a temperate forest site. *Journal of Geophysical Research: Atmospheres* (1984–2012),  
472 111(D16)

473 Hammerle, A., Haslwanter, A., Tappeiner, U., Cernusca, A., & Wohlfahrt, G. (2008). Leaf area controls on energy  
474 partitioning of a temperate mountain grassland. *Biogeosciences (Online)*, 5(2).

475 Honaker, J., et al. (2011). "Amelia II: A program for missing data." *Journal of statistical software* 45(7): 1-47.

476 Kolle, O., & Rebmann, C. (2007). EddySoft: Dokumentation of a Software Package to Acquire and Process Eddy  
477 Covariance Data.

478 Kutsch, W., Hanan, N., Scholes, R., McHugh, I., Kubheka, W., Eckhardt, H., & Williams, C. (2008). Response  
479 of carbon fluxes to water relations in a savanna ecosystem in ~~sSouth~~ ~~afriea~~Africa. *Biogeosciences Discussions*,  
480 5(3), 2197-2235.

481 Li, S., Eugster, W., Asanuma, J., Kotani, A., Davaa, G., Oyunbaatar, D., & Sugita, M. (2006). Energy partitioning  
482 and its biophysical controls above a grazing steppe in central ~~mongolia~~Mongolia. *Agricultural and Forest*  
483 *Meteorology*, 137(1), 89-106.

484 Li, Y., Liu, S., Wang, S., Miao, Y., & Chen, B. (2014). Comparative study on methods for computing soil heat  
485 storage and energy balance in arid and semi-arid areas. *Journal of Meteorological Research*, 28, 308-  
486 322.

487 Liu, S., Xu, Z., Wang, W., Jia, Z., Zhu, M., Bai, J., & Wang, J. (2011). A comparison of eddy-covariance and  
488 large aperture scintillometer measurements with respect to the energy balance closure problem. *Hydrology and*  
489 *Earth System Sciences*, 15(4), 1291-1306.

490 Ma, Y., Wang, Y., Wu, R., Hu, Z., Yang, K., Li, M., . . . Chen, X. (2009). Recent advances on the study of  
491 atmosphere-land interaction observations on the ~~tibetan~~[Tibetan](#) plateau. *Hydrology and Earth System Sciences*,  
492 13(7), 1103-1111.

493 Mauder, M., Jegede, O., Okogbue, E., Wimmer, F., & Foken, T. (2007). Surface energy balance measurements at  
494 a tropical site in ~~West africa~~[Africa](#) during the transition from dry to wet season. *Theoretical and Applied*  
495 *Climatology*, 89(3-4), 171-183.

496 Sánchez, J., Caselles, V., & Rubio, E. (2010). Analysis of the energy balance closure over a FLUXNET boreal  
497 forest in Finland. *Hydrology and Earth System Sciences*, 14(8), 1487-1497.

498 Scholes, R., Gureja, N., Giannecchini, M., Dovie, D., Wilson, B., Davidson, N., . . . Freeman, A. (2001). The  
499 environment and vegetation of the flux measurement site near ~~skukuza~~[Skukuza](#), ~~kruger~~[Kruger](#) ~~n~~[National](#) ~~p~~[Park](#).  
500 *Koedoe-African Protected Area Conservation and Science*, 44(1), 73-83.

501 Scholes, R. J., Bond, W. J., & Eckhardt, H. C. (2003). Vegetation dynamics in the ~~kruger~~[Kruger](#) ecosystem *The*  
502 *Kruger Experience*. Island Press.

503 Shugart, H., Macko, S., Lesolle, P., Szuba, T., Mukelabai, M., Dowty, P., & Swap, R. (2004). The SAFARI 2000–  
504 Kalahari transect wet season campaign of year 2000. *Global Change Biology*, 10(3), 273-280.

505 Stull, R. B. (2012). *An introduction to boundary layer meteorology* (Vol. 13): Springer Science & Business Media.

506 Su, H., Schmid, H. P., Grimmond, C., Vogel, C. S., & Oliphant, A. J. (2004). Spectral characteristics and  
507 correction of long-term eddy-covariance measurements over two mixed hardwood forests in non-flat  
508 terrain. *Boundary-Layer Meteorology*, 110(2), 213-253.

509 Twine, T. E., Kustas, W., Norman, J., Cook, D., Houser, P., Meyers, T., . . . Wesely, M. (2000). Correcting eddy-  
510 covariance flux underestimates over a grassland. *Agricultural and Forest Meteorology*, 103(3), 279-300.

511 Von Randow, C., Manzi, A., Kruijt, B., De Oliveira, P., Zanchi, F., Silva, R., . . . Waterloo, M. (2004).  
512 Comparative measurements and seasonal variations in energy and carbon exchange over forest and pasture in  
513 south west ~~amazonia~~[Amazonia](#). *Theoretical and Applied Climatology*, 78(1-3), 5-26.

514 Wilczak, J. M., Oncley, S. P., & Stage, S. A. (2001). Sonic anemometer tilt correction algorithms. *Boundary-*  
515 *Layer Meteorology*, 99(1), 127-150.

516 Williams, C. A., Hanan, N., Scholes, R. J., & Kutsch, W. (2009). Complexity in water and carbon dioxide fluxes  
517 following rain pulses in an [African](#) savanna. *Oecologia*, 161(3), 469-480.

518 Wilson, K., Goldstein, A., Falge, E., Aubinet, M., Baldocchi, D., Berbigier, P., . . . Field, C. (2002). Energy  
519 balance closure at FLUXNET sites. *Agricultural and Forest Meteorology*, 113(1), 223-243.

520 Xin, X., & Liu, Q. (2010). The two-layer surface energy balance parameterization scheme (TSEBPS) for  
521 estimation of land surface heat fluxes. *Hydrology and Earth System Sciences*, 14(3), 491-504.

522 Yuling, F. (2005). Energy balance closure at ChinaFLUX sites.

523 [Zuo, J. Q., Wang, J. M., Huang, J. P., Li, W., Wang, G., & Ren, H. \(2011\). Estimation of ground heat flux and its](#)  
524 [impact on the surface energy budget for a semi-arid grassland. \*Sci Cold Arid Region\*, 3, 41-50.](#)

525

526

527

**Table 1: Measurements taken and instruments used at Skukuza flux tower**

Instrument	Model/ brand	Measurement
Sonic anemometer	Gill Instruments Solent R3, Hampshire, England	3-dimensional, orthogonal components of velocity (u, v, w ( $\text{ms}^{-1}$ )), <u>sonic temperature</u>
Closed path gas analyser	IRGA, LiCOR 6262, LiCOR, Lincoln	Water vapor, carbon dioxide concentrations
Radiometer	Kipp and Zonen CNR1, Delft, The Netherlands	Incoming and outgoing longwave and shortwave radiation
HFT3 plates	Campbell Scientific	Soil heat flux at 5 cm depth with 3 replicates, i.e. two under tree canopies and one on open space
Frequency domain reflectometry probes	Campbell Scientific CS615, Logan, Utah	Volumetric soil moisture content with two in the Acacia – dominated soils downhill of the tower at 3, 7, 16, 30, and 50 cm, and another two at 5, 13, 29, and 61 cm in the Combretum – dominated soils uphill

528

529

530

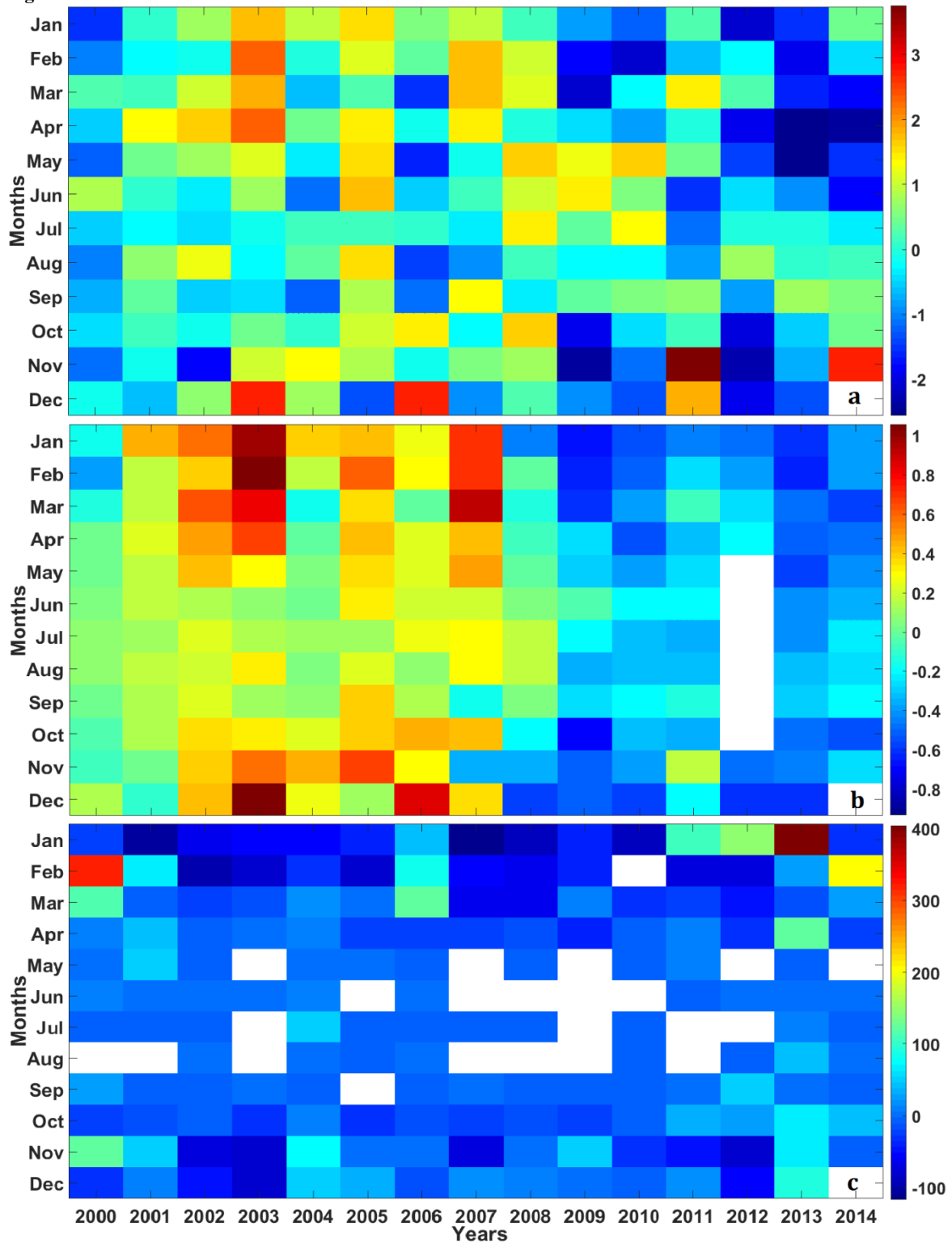
**Table 2: Statistical summary of annual values of the energy balance components**

Year	% data completion		H	LE	G	Rn
2000	14.16	Max	470.31	422.89	191.53	817.60
		Min	-139.77	-72.43	-61.60	-95.93
		Mean	45.82	36.11	5.32	91.46
2001	12.78	Max	790.82	513.09	292.87	899.90
		Min	-159.87	-85.95	-90.27	-116.58
		Mean	58.56	43.68	9.27	128.27
2002	17.77	Max	415.93	174.07	171.93	583.30
		Min	-117.66	-89.16	-86.00	-122.21
		Mean	61.35	10.29	4.10	90.72
2003	41.50	Max	556.21	308.71	217.60	879.30
		Min	-92.99	-97.81	-106.23	-116.04
		Mean	58.15	21.68	6.17	94.53
2004	28.21	Max	505.36	498.10	129.96	925.30
		Min	-150.08	-89.07	-69.76	-5.88
		Mean	56.46	17.99	7.97	156.10
2005	35.37	Max	606.28	737.43	288.20	933.20
		Min	-130.40	-97.00	-107.37	-4.92
		Mean	51.43	17.82	0.99	159.09
2006	7.59	Max	583.66	331.25	335.30	1003.30
		Min	-72.45	-119.09	-72.80	-6.56
		Mean	84.67	35.94	19.69	247.70
2007	48.77	Max	552.93	426.34	340.67	1011.30
		Min	-131.40	-130.79	-129.70	-6.71
		Mean	59.04	14.32	4.14	169.84
2008	54.30	Max	616.43	439.76	238.57	1038.50
		Min	-140.13	-144.97	-104.60	-5.91
		Mean	63.06	26.30	6.22	191.26
2009	42.69	Max	551.34	776.62	328.93	1060.50
		Min	-96.68	-135.43	-94.20	-155.90
		Mean	55.42	96.54	6.87	207.77
2010	57.65	Max	626.68	624.38	199.33	888.00
		Min	-173.11	-135.62	-66.35	-180.70
		Mean	57.23	52.54	3.74	105.10
2011	41.34	Max	591.16	688.46	171.27	832.00
		Min	-135.77	-127.02	-58.59	-96.50
		Mean	63.88	73.11	1.75	127.94
2012	27.62	Max	572.11	566.88	185.80	899.00
		Min	-171.83	-148.49	-50.92	-99.69
		Mean	59.25	52.49	2.16	111.31
2013	67.97	Max	570.79	665.48	146.03	845.58
		Min	-197.40	-149.10	-55.36	-107.70
		Mean	50.25	38.63	-1.22	92.80
2014	28.66	Max	533.46	726.31	89.50	893.00
		Min	-238.65	-134.39	-33.36	-89.70
		Mean	59.37	69.55	1.18	147.30

534 Figures

535

536 Figures



537

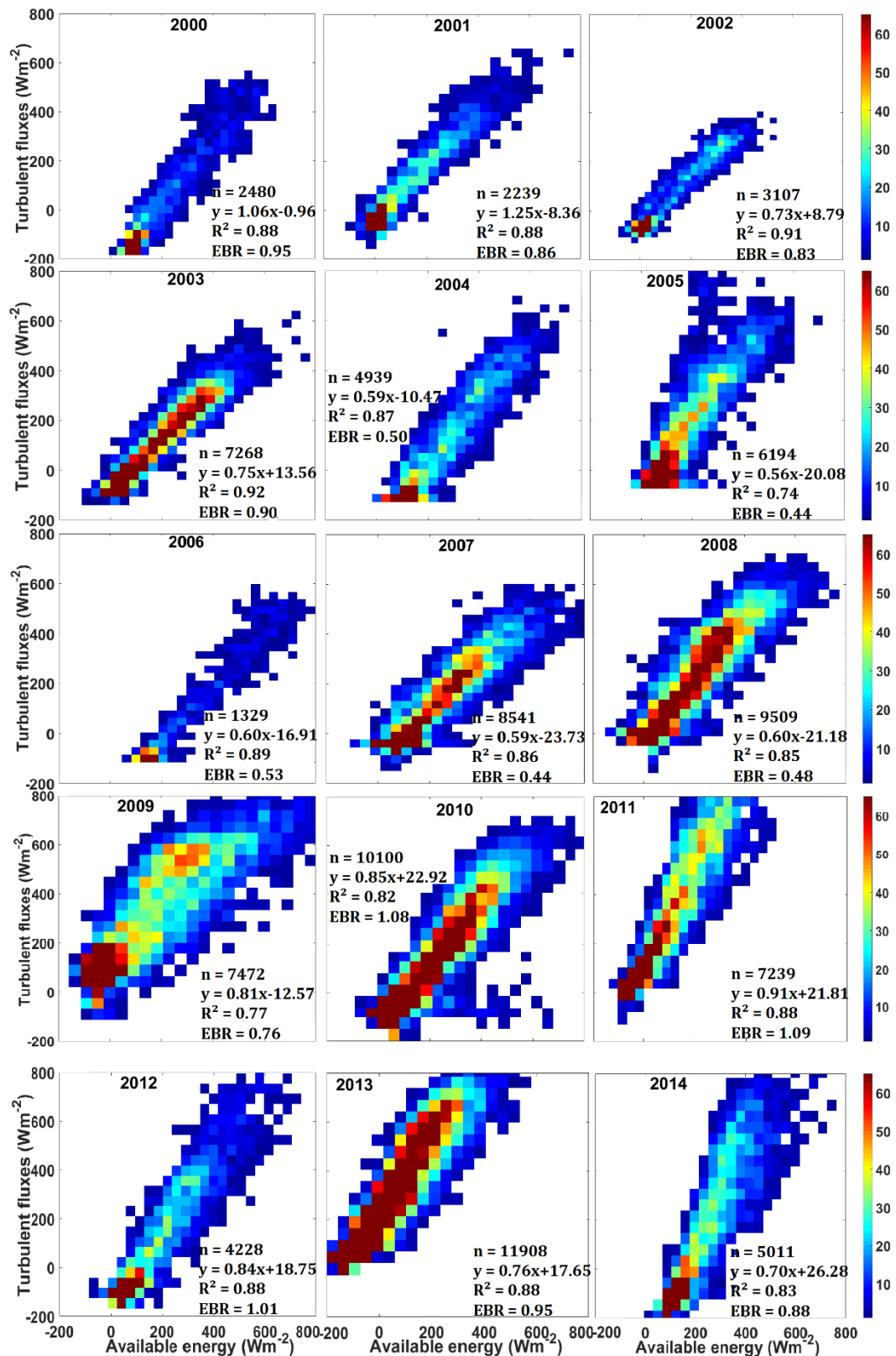
538

539

Figure 1: Summaryies of daily-mean monthly anomalies of (a) average air temperature, (b) average VPD, and (c) total rainfall from 2000 to 2014

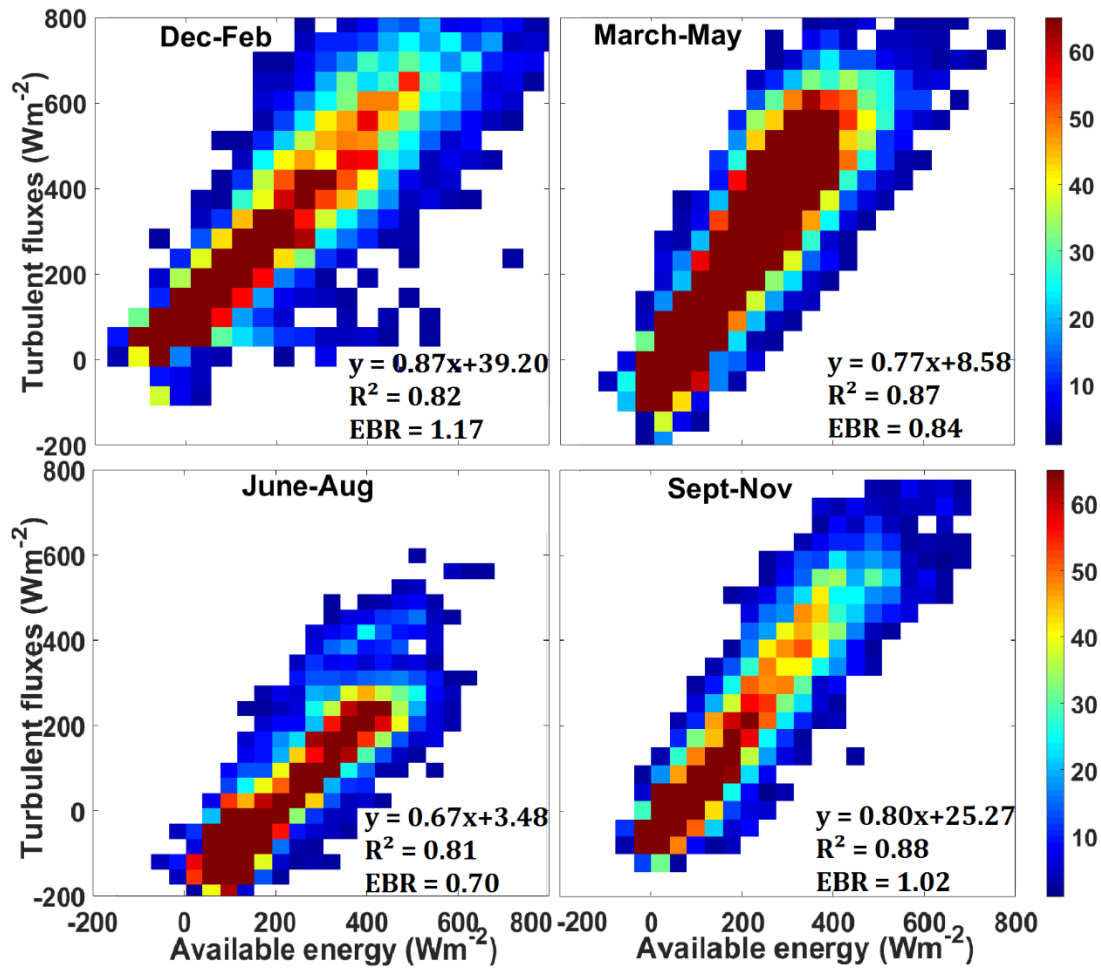
540





541  
542  
543  
544

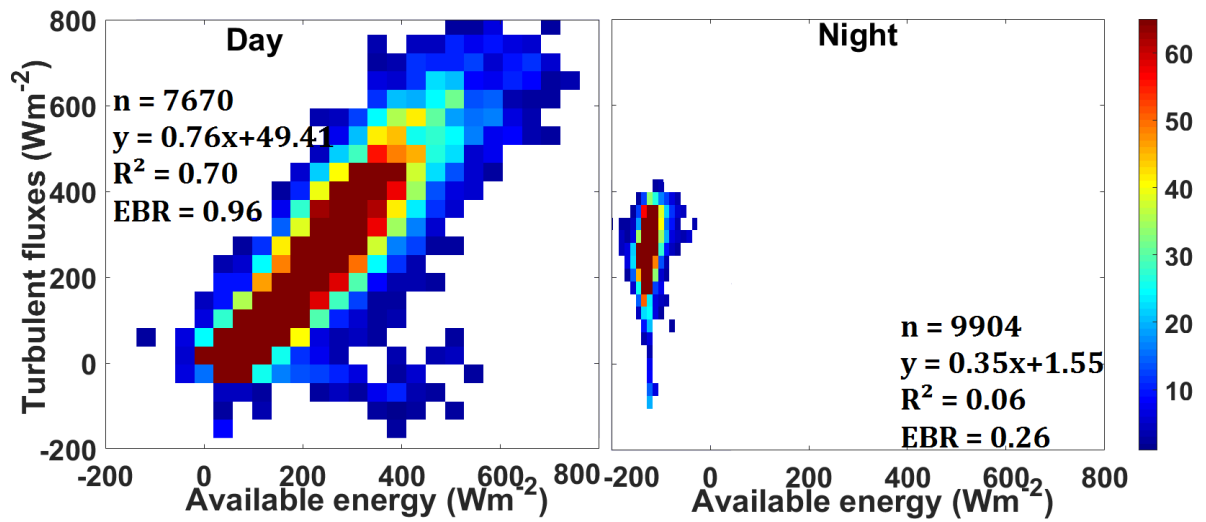
Figure 2: 15-year series of annual regression analysis of turbulent (sensible and latent) heat fluxes against available energy (net radiation minus ground-conduction heat flux) from 2000 to 2014 at Skukuza, (SA). The colour bars represent the count of EBR values.



545

546 Figure 3: Seasonal turbulent fluxes (H+LE) correlation to available energy (Rn-G) for Skukuza flux tower from  
 547 summer(Dec-Feb), autumn (March-May), winter (June-Aug), spring (Sept-Nov). The colour bars represent the count  
 548 of EBR values

549

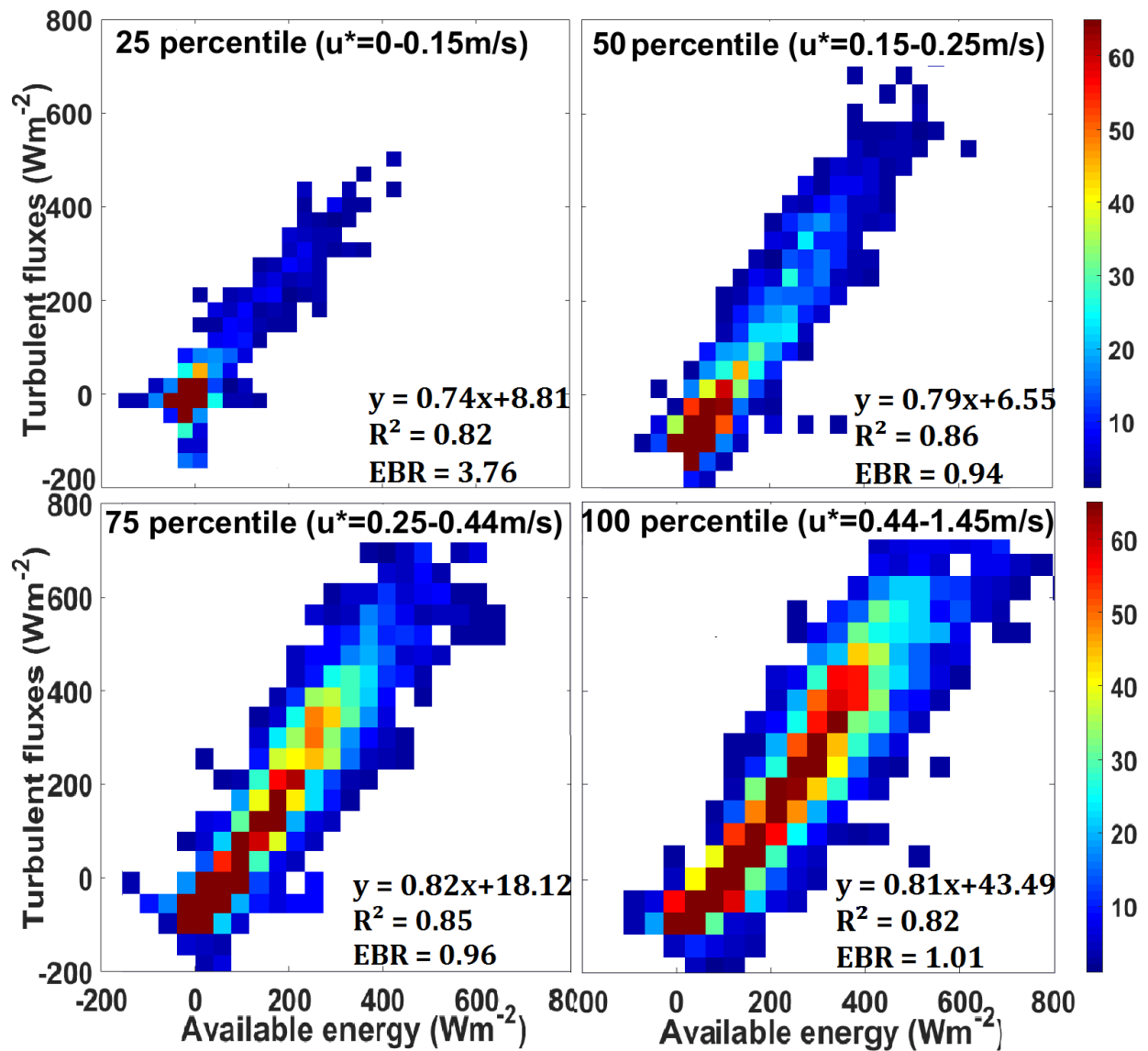


550  
551  
552

Figure 4: Turbulent fluxes correlation ~~to available~~ to available energy for daytime (a) and night-time (b), using the full (2000-2014) 15-year available data series. The colour bars represent the count of EBR values

553

554

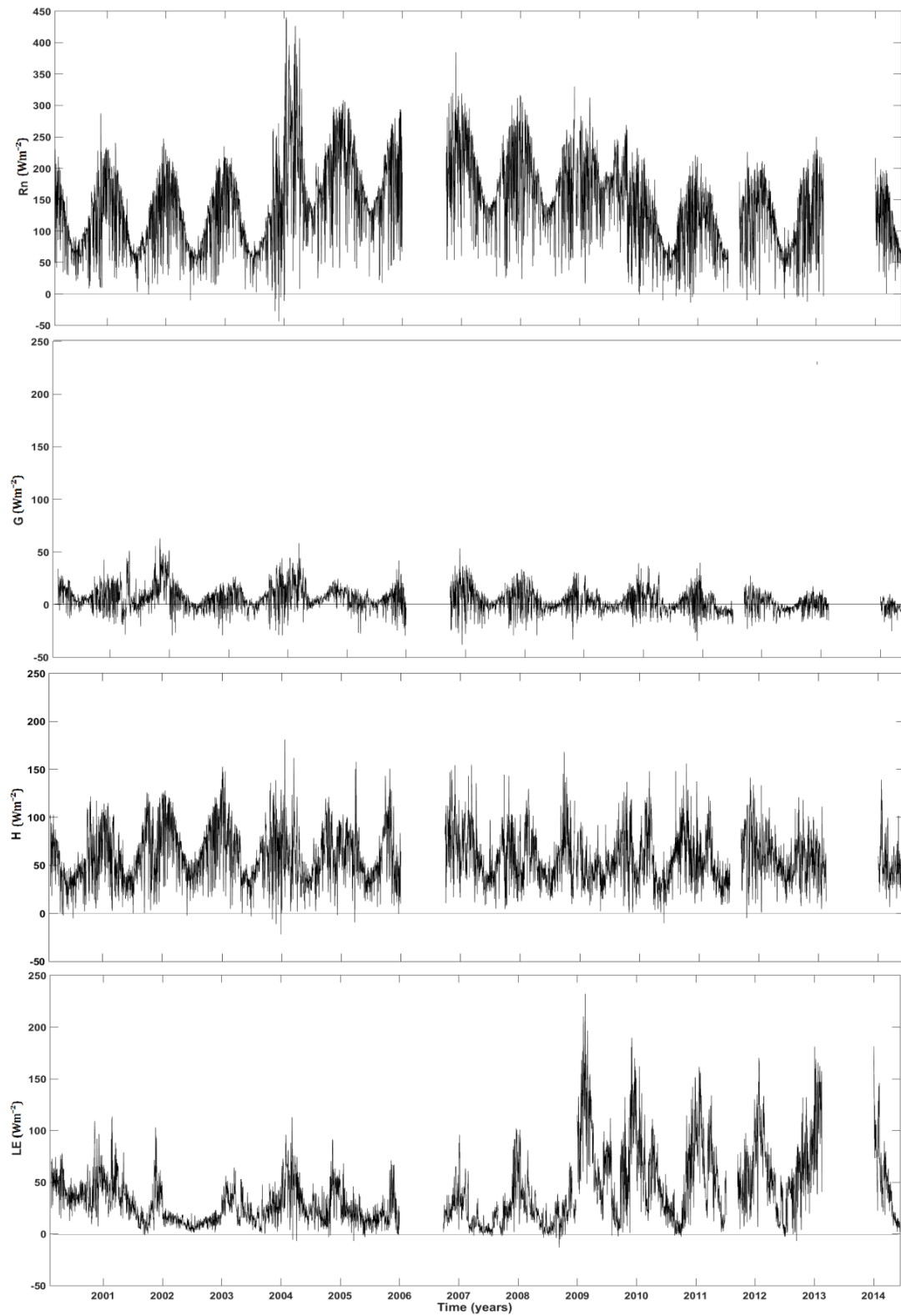


555  
556  
557

Figure 5: OLS and EBR evaluations at different friction velocity sorted at four quartiles. The colour bar represents the count of EBR values. The colour bars represent the count of EBR values.

558

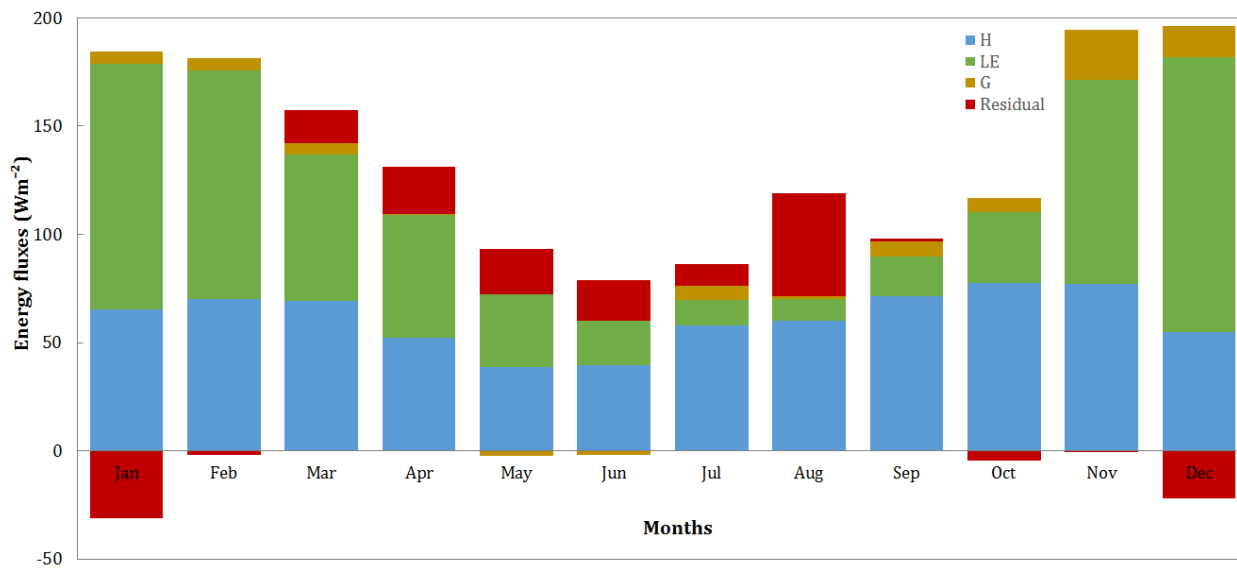
559



560  
 561  
 562  
 563

**Figure 6: Time series of daily mean surface energy balance component fluxes from 2000 to 2014 at Skukuza flux tower site (SA)**

564



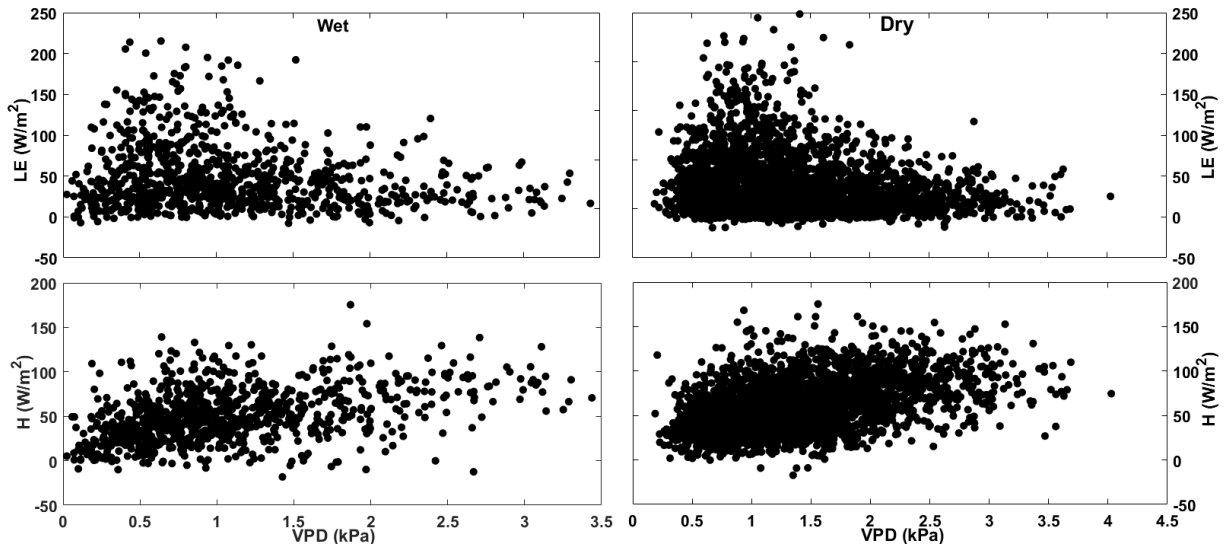
565

566

567

Figure 7: 15-year (2000-2014) monthly means of surface energy balance fluxes of Skukuza flux tower site (SA), highlighting the partitioning of Rn

568

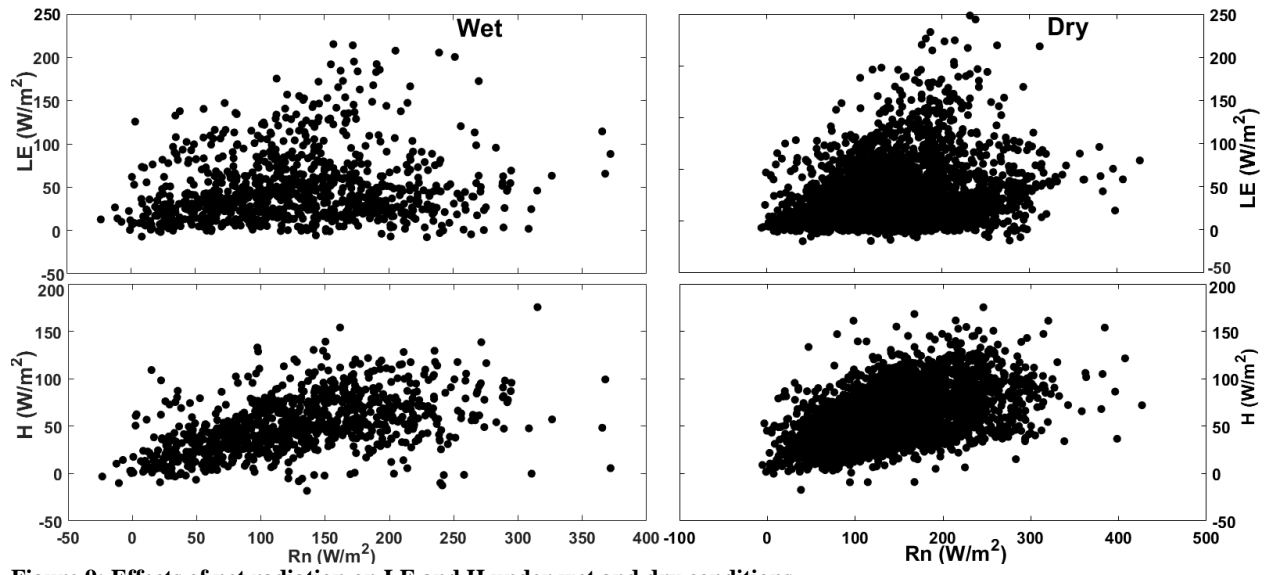


569

570

Figure 8: Relationship between the fluxes and VPD under wet and dry conditions

571



572  
573

Figure 9: Effects of net radiation on LE and H under wet and dry conditions

574